Thermal conductivity of monolithic synthetic hard carbons as a function of pyrolysis temperature

M. Wiener[1], G. Reichenauer[1,2], F. Hemberger[2], H.-P. Ebert[2]

[1]*Physics Department, Würzburg University, Am Hubland, 97074 Würzburg, Germany*
Email: matthias.wiener@zae.uni-wuerzburg.de
[2]*Bavarian Center for Applied Energy Research, Am Hubland, 97074 Würzburg, Germany*

Abstract. Amorphous carbon samples with a total porosity of about 85% were synthesized via pyrolysis of sol-gel derived resin precursors. Since the pores in the samples investigated have dimensions of a few tens of nanometers only, the gaseous contribution to the thermal conductivity is largely suppressed at ambient pressure. Values for the total thermal conductivity as low as 0.054 $W(mK)^{-1}$ at 300°C are detected. However, the pyrolysis temperature has a great impact on the contribution of the solid backbone to the total thermal conductivity. From the same precursor a series of samples was prepared via pyrolysis at temperatures ranging from 800 to 2500°C. The thermal conductivity of this series of carbons at 300°C under vacuum increases by a factor of about 8 if the pyrolysis temperature is shifted from 800 to 2500°C. To elucidate the reason for this strong increase the infrared radiative properties, the electrical conductivity, the macroscopic density, the microcristallite size, the sound velocity and the inner surface of the samples were determined. Evaluation of the experimental data yields only a negligible contribution from radiative heat transfer and electronic transport to the total thermal conductivity. The main part of the increasing thermal conductivity therefore has to be attributed to an increasing phonon mean free path in the carbons prepared at higher pyrolysis temperatures. However, the phonon mean free path does not match directly the in-plane microcristallite size of the amorphous carbon. The in-plane microcristallite size rather represents an upper limit for the phonon mean free path. Hence, the limiting factor for the heat transport via phonons has to be defects within the carbon microcristallites which are partially cured at higher temperatures.

Keywords : thermal conductivity, pyrolysis temperature, aerogels, amorphous carbon, mean free path, microcrystallites

1 Introduction

The amorphous carbons investigated in this study were derived via pyrolysis of highly porous resorcinol formaldehyde resins according the sol gel route first published by R. W. Pekala [1]. This type of material is also called carbon aerogels or xerogels. Besides the application of carbon aerogels as electrodes in supercapacitors [2,3] or gas diffusion layers in fuel cells [4,5] they are promising materials for high temperature thermal insulation. The morphology of a typical carbon aerogel is shown in figure 1. The picture shows a network of interconnected spherical primary particles that defines an interconnected pore phase. By varying the synthesis parameters, i.e. by varying the composition of the starting solution and the process temperature of the sol-gel process, it is possible to tailor the particle and pore sizes in the range from a few nanometers up to some microns; applying ambient pressure drying of the gelled and cured resins porosities up to 85% can be achieved. This is the key for thermally stable materials with exceptionally small thermal conductivities. However, the thermal conductivity of this type of amorphous carbon depends significantly on the pyrolysis temperature applied. In the past, other authors have studied the effects of high temperature treatment on the properties of hard carbons. Hanzawa et al. and Soukup et al. [6,7] have investigated in detail the changes of microcristallite properties in carbon aerogels and glassy carbon, respectively. Lu et al. and Nilsson et al. [8,9] analyzed the thermal conductivity of carbon aerogels as a function of temperature, sample density and electrical conductivity, respectively. Bock et al. [10] investigated the thermal conductivity of carbon aerogels as a function of sample density and temperature as well as the in-plane microcristallite size and phonon mean free path as a function of the sample density.

In this work we systematically analyze the changes of material properties, like the electrical conductivity, the sample density, the microcristallite size, the sound velocity and the inner surface as a function of the pyrolysis temperature and their impact on the total thermal conductivity.

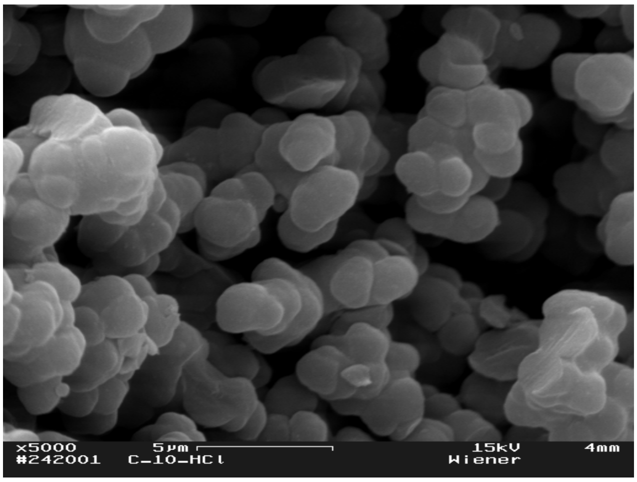

Figure 1. SEM micrograph showing the typical morphology of a monolithic carbon aerogel with particle sizes around 1µm and pore sizes in the 5µm range.

2 Experimental

2.1 Sample preparation

The series of amorphous carbon investigated in this work was derived via pyrolysis of the same organic precursor at different temperatures. The synthesis of carbon aerogels is described in detail elsewhere [11]. Briefly, the precursors were synthesized by adding sodium carbonate as a base catalyst to an aqueous solution of resorcinol and formaldehyde. The molar ratio of formaldehyde to resorcinol is 2:1 and the mass ratio of resorcinol and formaldehyde in the solution was chosen to yield a final density of about 300 kg/m^3. First the solution was filled in a vessel and sealed airtight; then it was exposed to 85°C for 24h for gelling and curing. Afterwards the pore liquid within the wet gel (essentially water) was replaced by ethanol (a liquid with lower surface tension) and the gel was dried at ambient conditions. The resulting organic aerogel was then cut into eight small cylinders of the same size (diameter = 21mm; height = 6mm). Each piece was finally pyrolized in an inert atmosphere at 800°C for the lowest and 2500°C for the highest final temperature, respectively (s. Table 1). A temperature ramp of 5°C/min was used; no dwell time was applied at the target temperature.

2.2 Sample Characterisation

Density

The density of each sample was calculated from its dimensions and weight measured after heat treatment.

Electrical Conductivity

The electrical conductivity was measured with a four wire setup in order to avoid contact resistance effects [3]. The current and voltage were measured with a HP 3457A multimeter. The voltage was tapped by two sharp stainless steel pins mounted onto a movable measuring head. For each sample three measurements were performed at different locations of the sample and the values were averaged to derive a mean value for the electrical conductivity.

Microcrystallite size

For the quantification of disordered graphitic structures and in particular for the characzterization of microcrystallite sizes in carbon materials Raman spectroscopy is a convenient method. The spectra were measured using the 488 nm line of an argon ion laser and the power of excitation was adjusted to about 70 µW in order to prevent the sample surface from degradation or heating during measurement. In the experiment a range in wave numbers from 700 cm^{-1} to 2000 cm^{-1} was covered. A typical Raman plot is shown in figure 2. There are two dominant bands in the spectrum, one at around 1360 cm^{-1} associated with edge planes of microcrystallites and the Raman-active $E_{2g}^{(2)}$ mode at 1582 cm^{-1} [12]. According to the empirical formula of Knight and White [13] it is possible to extract the in-plane micro crystallite size L_a via the following relationship

$$L_a(\text{Å}) = 44\,(I_{1582}/I_{1360}), \tag{1}$$

where I_{1360} and I_{1582} are the integrated intensities of the respective peaks. To determine the integrated intensities the two bands were fitted to a Breit-Wigner-Fano lineshape [14]:

$$I(\upsilon) = \frac{I_0[1+2(\upsilon-\upsilon_0)/q\Gamma]^2}{1+[2(\upsilon-\upsilon_0)/\Gamma]^2}, \tag{2}$$

where $I(\upsilon)$ is the intensity, υ_0 is the wave number at the peak, I_0 is the intensity at the peak position, Γ is the peak width at half-height and 1/q is a parameter accounting for the interactions between the discrete $E_{2g}^{(2)}$ mode and a Raman-active continuum (1/q=0 for Lorenzian lineshape) [14].

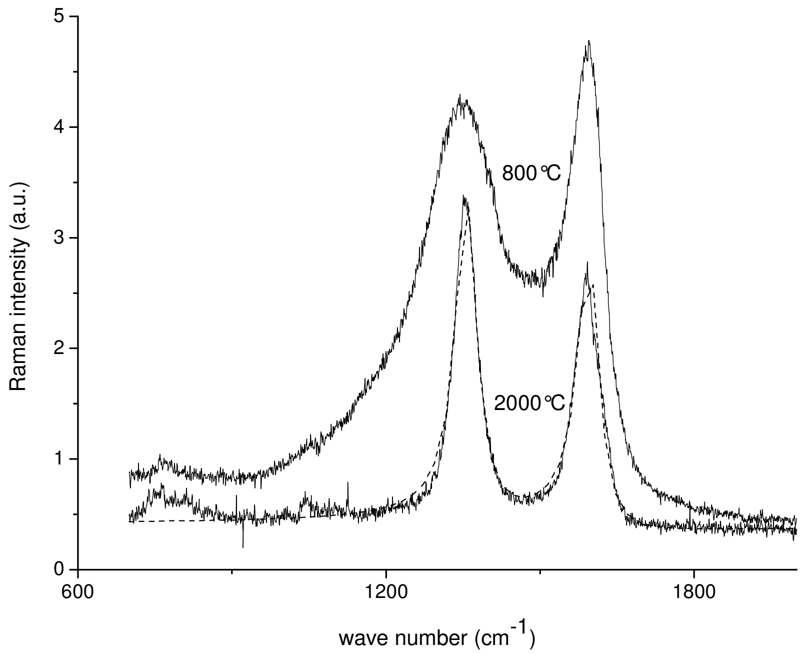

Figure 1. Raman spectra of carbon aerogels pyrolized at 800°C and 2000°C, respectively. The dashed line is a fit of equation (2) to the experimental data of the sample pyrolized at 2000°C.

Ultrasonic Velocity

The propagation of an ultrasonic signal across the sample was measured by a set-up consisting of a piezo transmitter operating at 0.5 MHz and a piezo receiver. The sample was clamped between the transmitter and the receiver and the time delay was monitored by a HP 54601A oscilloscope. The sound velocity then was calculated from sample dimension divided by time delay.

Extinction Coefficient

To determine the infrared-optical extinction coefficient the spectral–hemispherical transmittance T_{dh} and reflectance R_{dh} of the samples were measured by the integrating sphere method for wavelengths between 2 µm and 18µm. From T_{dh} and R_{dh} the scaled mass specific scattering coefficient s^* and the mass specific absorption coefficient a can be derived via the three-flux method [15]. Finally the specific extinction coefficient e can be calculated according to

$$e^* = a + s^*. \tag{3}$$

Surface area and pore volume

The surface area and pore volume of each sample was determined via N_2-Sorption measurements at 77K using a Micromeritics ASAP 2000 apparatus. Prior to adsorption the samples were degassed at 110°C under vacuum for at least 12 h. Figure 3 depicts a typical nitrogen adsorption/desorption isotherm of one of the carbons investigated.

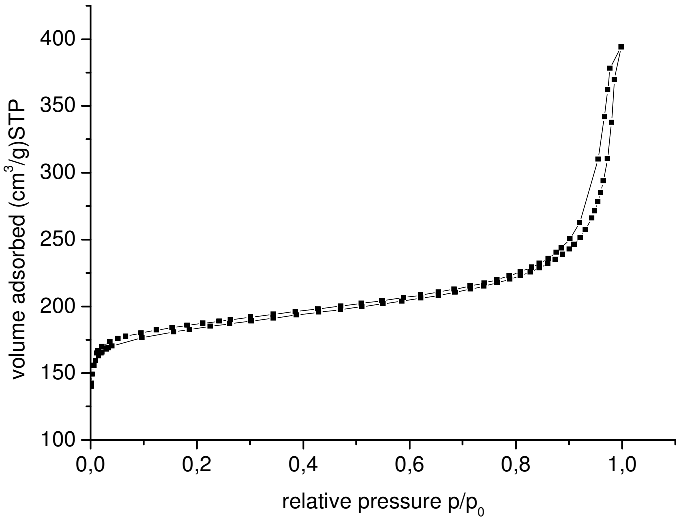

Figure 3. Nitrogen sorption isotherm of the carbon sample pyrolized at 1000°C.

By applying different evaluation methods it is possible to distinguish between "inner" surface of the sample due to micropores (< 2nm) and the "external" surface due to meso- or macropores (> 2nm), respectively. From the isotherm the total specific surface S_{BET} of the sample was calculated by applying the BET- method [16] in the relative pressures range between 0.1 and 0.26. In addition, the external surface S_{ext} (due to meso- or macropores) was determined from the slope of the linear region of the t-plot. The micropore surface S_{μ} was then calculated using $S_{\mu} = S_{\mathrm{BET}} - S_{\mathrm{ext}}$.

Thermal Conductivity

The thermal properties of the series of samples were determined by the laser flash method. The measurements were performed under vacuum at 300°C in order to exclude contributions due to gaseous conductivity and adsorbed molecules at the inner surface of the porous samples. The front side of the sample was thermally excited by a laser flash pulse (NdYaG-laser, 1064nm). The back side temperature was monitored by a MCT infrared detector as a function of time. The assembly of the laser flash apparatus used, is described in detail elsewhere [17]. From the time dependence of the signal the thermal diffusivity a is determined [18]. With known specific heat capacity c_p, the thermal conductivity λ of the material can be calculated from

$$\lambda(T,T_P) = a(T,T_P) \cdot \rho(T_P) \cdot c_p(T). \qquad (4)$$

Here T is the temperature at which the thermal measurement is performed and T_P is the temperature applied to the samples upon pyrolysis. The values for the specific heat c_p below 200°C were determined under argon by temperature modulated differential scanning calorimetry (MDSC) (figure 4); above 200°C literature values were used [19]. It can be seen that the two curves coincide in the range around 200°C.

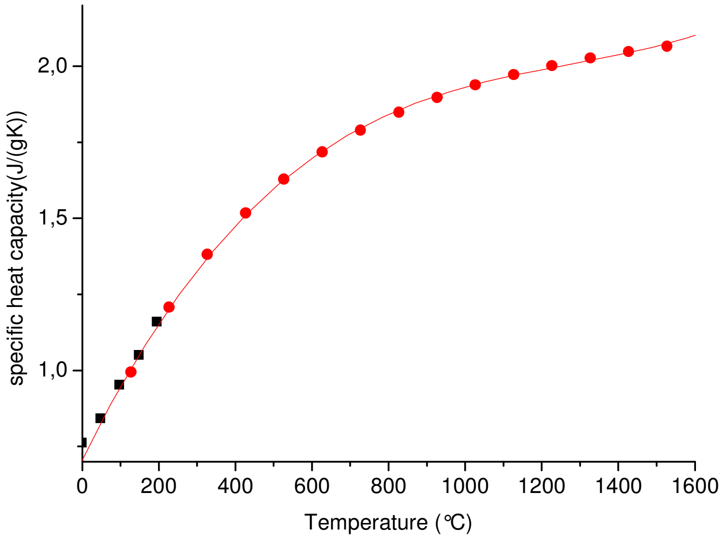

Figure 4. Specific heat capacity c_p as a function of temperature. (■) represent experimental values determined by dynamic difference calorimetry, (●) are data taken from literature [19].The line represents a polynomial fit to the data.

3 Theoretical background

Generally, the heat transport through a porous solid consists of a radiative, a gaseous and a solid contribution. The radiative thermal conductivity λ_{rad} can be calculated according to

$$\lambda_{rad} = \frac{16 \cdot \sigma \cdot n^2}{3 \cdot \rho \cdot e} \cdot T^3 . \tag{5}$$

Hereby σ is the Stefan-Boltzmann constant, $n \approx 2$ is the refractive index for carbon, T is the temperature, ρ is the sample density and e is the mass specific extinction coefficient (see equation (3)).

The solid thermal conductivity can be expressed in a first order approximation by the sum of electronic contribution λ_{el} and phononic contribution λ_{ph}, respectively. The electronic thermal conductivity for metals and semimetals can be described by the Wiedemann-Franz law [20]

$$\lambda_{el} = \sigma \cdot L \cdot T , \tag{6}$$

where σ is the electrical conductivity and L is the Lorentz number.

The phononic contribution to the thermal conductivity in the solid phase is given by [22]

$$\lambda_{ph} = \frac{1}{3} \cdot \rho \cdot c_v \cdot v_{ph} \cdot l \tag{7}$$

where $c_v \approx c_p$, v_{ph} is an average phonon velocity and l is the mean free path of the phonons.

4 Results

Density

The density of the series of carbons was determined as a function of pyrolysis temperature (figure 5). The experimental results for the different samples vary between *301 kg/m*^{3} and *323 kg/m*^{3}. However, within the given uncertainty of 4% the density can be assumed to be independent of the pyrolysis temperature and is therefore set to (312±12) kg·m^{-3}in the further course of this paper.

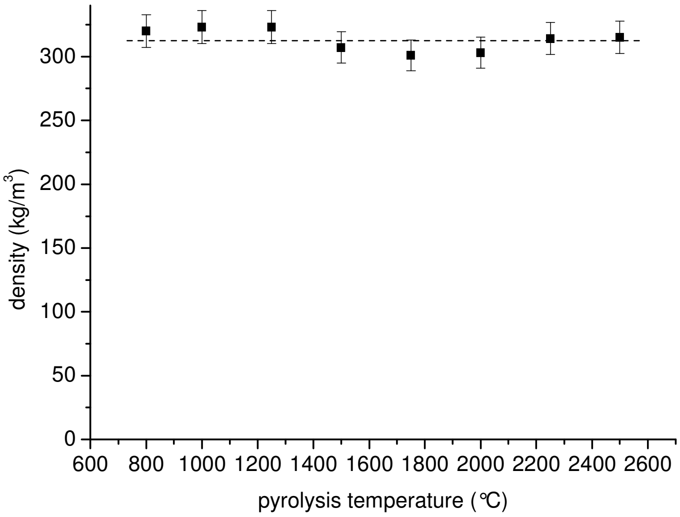

Figure 5. Sample densities as a function of temperature treatment. The dashed line corresponds to the mean value of all samples.

Electrical conductivity

The electrical conductivities of the carbons as a function of pyrolysis temperature are shown in figure 6. For samples pyrolized up to 1250°C the electrical conductivity rises significantly from 3 S·cm^{-1} at 1000°C to about 6.5 S·cm^{-1}, beyond 1250°C the electrical conductivity increases moderately to about 9 S·cm^{-1}. These values correspond to the electrical conductivities reported by Lu et al. for supercritically dried carbon aerogels with comparable densities [8]. Soukup et al. [7] also observed a tendency to saturation in electrical conductivity for heat treatment temperatures above 1800°C when investigating glassy carbons, the dense version of carbon aerogels (figure 6).

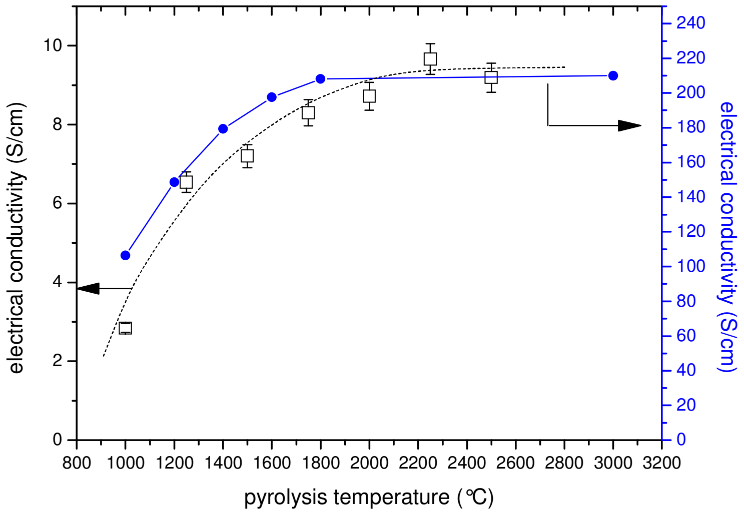

Figure 6. Electrical conductivity of carbon aerogels as a function of pyrolysis temperature (□). The dashed line is a guide to the eye. For comparison values determined by [7] for glassy carbon are plotted (●). Due to the higher density of the glassy carbon (a factor of about 5 compared to the aerogel) the electrical conductivity is significantly increased (note the corresponding second axis on the right).

Microcrystallite size

Primary particles building the skeleton of hard carbons consist of a disordered system of graphene microcrystallites (house of cards model) [14]. The in-plane microcrystallite sizes L_a as determined via equation (1) from Raman data are given in figure 7. The average in-plane microcrystallite dimension L_a expands from 28Å for a carbon sample pyrolyzed at 800°C to 47Å for a sample pyrolyzed at 2500°C.

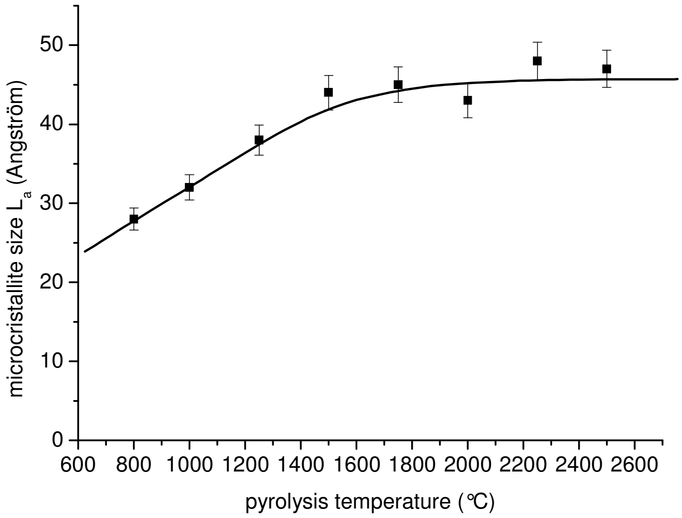

Figure 7. In-plane microcrystallite size L_a of amorphous carbon samples as a function of pyrolysis temperature calculated from Raman data. The full line is a guide to the eye.

Ultrasonic velocity

Morphological or structural changes caused by the temperature treatment affect the elastic properties and hence the sound velocity. In figure 8 the sound velocities of the samples pyrolized at temperatures between 800℃ and 2500℃ are shown.

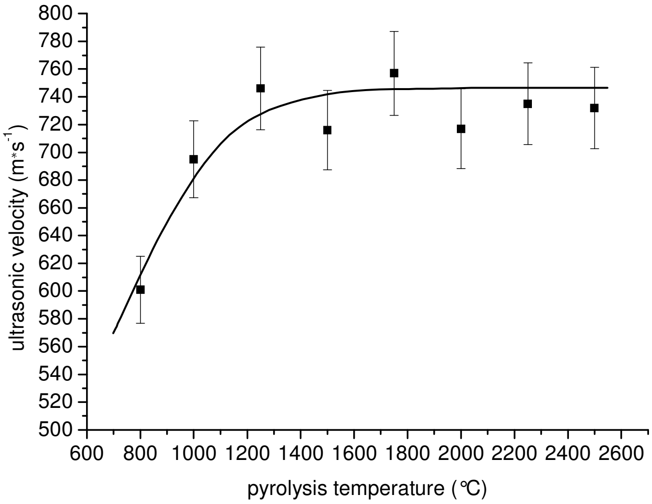

Figure 8. Ultrasonic velocity as a function of treatment temperature. Note that the zero is strongly suppressed. The full line is a guide to the eye.

The sound propagation velocity of the sample pyrolized at 800℃ is about 600 m·s^{-1}. For the sample treated at 1000℃ the sound velocity rises to 700m/s and approaches about 720 m·s^{-1} for treatment temperatures of 1250℃ and above.

IR-optical extinction coefficient

The measurements were performed with a Fourier transform infrared spectrometer combined with an external integrating sphere. The results for the scaled spectral scattering coefficient s^* and absorption coefficient a are shown in figure 9a for the two samples pyrolized at 800℃ and 2500℃. Using a suitable averaging procedure ("Rosseland" average) the mass specific extinction coefficient can be derived (figure 9b).

Surface area and pore size

When increasing the pyrolysis temperature from 800℃ to 1000℃ nitrogen sorption yields an increase in total surface S_{BET} from about 530 m^2·g^{-1} to 570 m^2·g^{-1} . Higher pyrolysis temperatures result in a decrease in S_{BET} down to about 150 m^2·g^{-1} . The micropore surface area S_{μ} shows the same trend indicating that the BET surface area is dominated by adsorption in micropores. In contrast, the external surface S_{ext} is almost unaffected by the treatment in the temperature range from 800℃ to 2500℃ (see figure 10).

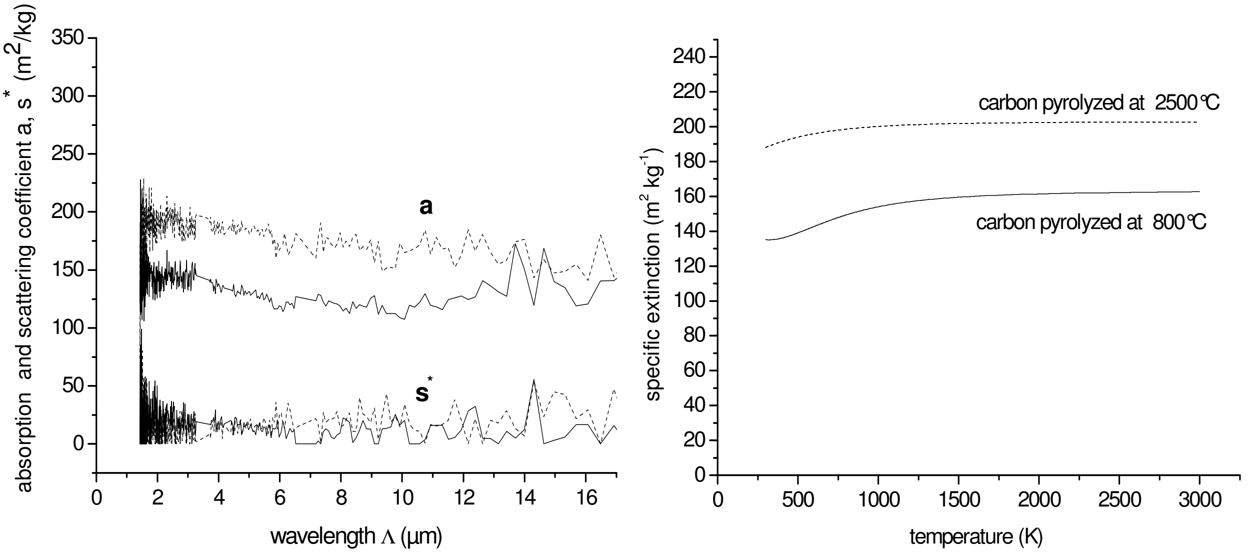

(a) (b)

Figure 9. (a) Scaled specific scattering coefficient s^* and specific absorption coefficient a vs. wavelength Λ for samples pyrolized at 800°C (—) and 2500°C (-----), respectively. (b) Mass specific extinction coefficient for the two samples; the data were derived via Rosseland averaging of the spectral data.

Thermal conductivity

Figure 11 depicts the values of thermal conductivity at 300°C calculated via equation (4) from the laser flash results. The thermal conductivity for the sample pyrolyzed at 800°C is 0.05 $W(m\ K)^{-1}$ at 300°C; the conductivity increases continuously with the treatment temperature to 0.42 $W(mK)^{-1}$ for the sample pyrolyzed at 2500°C. Figure 12 shows the thermal conductivity λ of a carbon sample pyrolized at 2000°C as a function of temperature. The experimental data were fitted with a linear superposition of a phonon, electronic and radiative heat transfer ($\lambda_{total} = \lambda_{ph} + \lambda_{rad} + \lambda_{el} = \alpha \cdot C_P(T) + \beta \cdot T^3 + \gamma \cdot T$); the temperature dependence of the respective components is given by Eqs. (5) through (7). Figure 12 clearly exhibits that the thermal transport below 1000°C is dominated by the conductivity of the solid phase. The electronic contribution is found to be negligible in the range investigated.

The fit parameters α and β are found to be 0.19 g $(m{\cdot}s)^{-1}$ and $1.8{\cdot}10^{-11}$ W $(m{\cdot}K^4)^{-1}$, respectively. Using equation (7) α yields a mean free path of 25 Å . The extinction coefficient determined from parameter β via equation (5) is 230 $m^2{\cdot}kg^{-1}$; this value is about a factor of 1.6 higher than the one determined via IR-spectroscopy (figure 9); this relatively large discrepancy, however, is not indicating a systematic deviation since the experimental temperature range (figure 12) is just too small to allow for a high enough accuracy in the extraction of the radiative contribution.

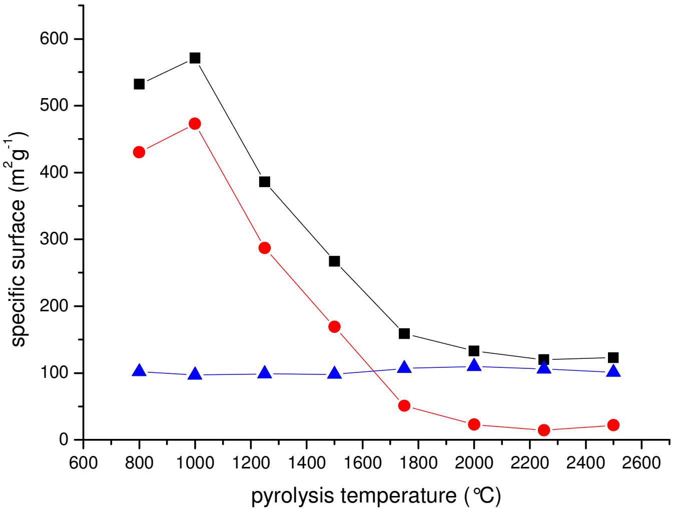

Figure 10. Specific surface area as a function of pyrolysis temperature as derived from nitrogen sorption measurements: S_{BET}(■), S_{μ} (●), S_{ext} (▲).

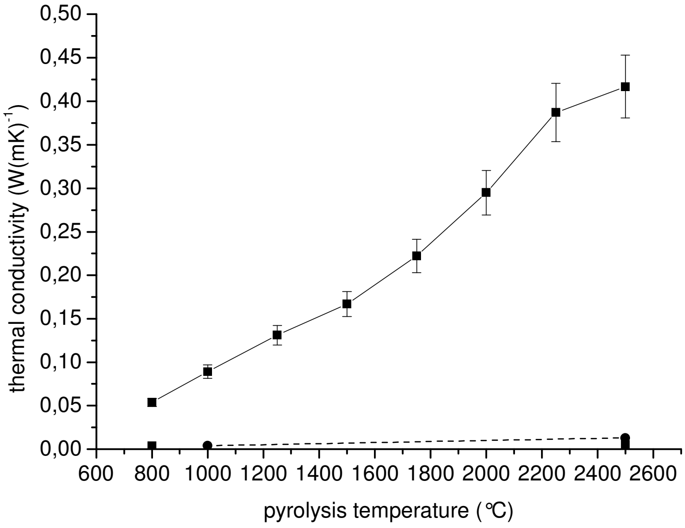

Figure 11. The full line shows the thermal conductivity of carbon aerogels measured at 300°C under vacuum and pyrolized at temperatures between 800°C and 2500°C. The data were calculated from the thermal diffusivities derived via laser flash measurements. The dashed line corresponds to the electrical contribution to the thermal conductivity calculated via equation (6). The radiative contribution determined via equation (5) is too small to be visible in this representation.

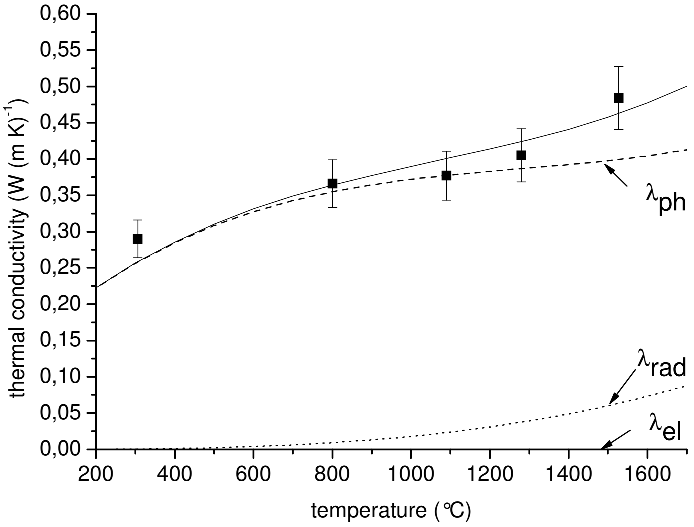

Figure 12. Thermal conductivity as a function of temperature for the carbon sample pyrolized at 2000°C. The full line is a fit of $\lambda_{total} = \lambda_{ph} + \lambda_{rad} + \lambda_{el}$ to the experimental data (see also equation (5) through (7)).The dashed line represents the solid conductivity. The dotted line indicates the contribution due to radiative heat transfer. The electronic contribution is too small to be visible in this representation.

All experimentally determined data are summarized in Table 1.

Table 1. Summary of experimentally determined data for the carbon samples pyrolized at temperatures between 800°C and 2500°C.

Pyrolysis Temperature /°C	Density / kg m^{-3}	Electrical Conductivity / S·cm^{-1}	Micro-Crystallite Size L_a / Angström	Ultrasonic Velocity / m·s^{-1}	S_{BET} / m^2 g^{-1}	S_{ext} / m^2 g^{-1}	S_{mic} / m^2 g^{-1}	Thermal Diffusivity a / mm^2 s^{-1}
800	320	--	28	601	532	102	430	0.126
1000	323	2.84	32	695	571	97	473	0.206
1250	323	6.54	38	746	386	99	287	0.305
1500	307	7.2	44	716	267	98	169	0.415
1750	301	8.3	45	757	159	107	51	0.550
2000	303	8.72	43	717	133	110	23	0.725
2250	314	9.66	48	735	120	106	14	0.925
2500	315	9.19	47	732	123	101	22	0.990

5 Discussion

The heat transport through a porous solid consists of a radiative, a gaseous and a solid contribution. A change of thermal conductivity with pyrolysis temperature (figure 11) in the series of samples investigated caused by a change of the gaseous contribution can be excluded because the measurements were performed under vacuum.

The values calculated for the radiative contribution to the thermal conductivity at 300°C are found to be between 0.005 W(m·K)$^{-1}$ (e ≈ 140 m^2 kg^{-1}; see figure 9) for the sample pyrolyzed at 800°C and 0.004W(m·K)$^{-1}$ (e ≈ 190 m^2 kg^{-1}; see figure 9) for the sample pyrolyzed at 2500°C. Both values are small compared to the total thermal conductivity (figure 11). This is also confirmed by the thermal conductivity measured as a function of temperature for the aerogel pyrolized at 2000°C (figure 12): The onset for the T^3-increase characteristic for radiative heat transfer (which is expected for a temperature independent extinction) first shows above 1250 °C. Therefore the contribution of radiation can not be responsible for the increase of the thermal conductivity at 300°C.

The change in thermal conductivity therefore has to be due to changes in the solid phase. However, modifications of the morphology of the porous carbon like sintering processes affecting the meso- or macroporosity obviously do not take place since otherwise the external surface of the samples investigated would not be constant (see figure 10). Similarly, the change in IR-extinction (figure 9) is mainly due to absorption while the scattering component that reflects the morphological characteristics of the samples is essentially unaffected by the pyrolysis temperature. In contrast, a modification of the solid on a length scale of 2 nm or below is obvious by the variation of the micropore surface S_μ determined by nitrogen sorption measurements (see figure 10) and the changes of the microcrystallite size (figure 7).

Generally, the solid thermal conductivity can contain both, electronic and phonic contributions. According to [8] the Wiedemann-Franz law (equation(6)) should be applicable to the type of carbon samples investigated here. The values of the electrical contribution to the thermal conductivity calculated by equation (6) yield values between 0.004 W/mK for the sample heat treated at 1000°C and 0.013 W/mK for the sample heat treated at 2500°C. The value for 1000°C corresponds to that one found out by Lu et al. [8] for a sample with similar density pyrolized at 1050°C. Although there is an obvious increase of the electrical contribution to the thermal conductivity caused by heat treatment, this contribution represents only a small effect compared to the experimental values for the thermal conductivity (Figs. 11 and 12).

The phononic thermal conductivity can be described by the phonon diffusion model (equation (7)). Assuming that the experimentally determined sound velocity v corresponds to the propagation velocity of the acoustic phonons v_{ph} within a solid, the phonon mean fee path l can be calculated from equation (4) according to

$$l = \frac{3a}{v} . \qquad (8)$$

Via equation (8) values for the mean free path l between 6 Å and 41 Å are obtained when the pyrolysis temperature is increasing from 800°C to 2500°C (figure 13). These values correspond approximately to the data mentioned in [10]. However, in contrast to reference [10] the mean free paths l calculated in this work are without exception smaller than the microcrystallite size L_a determined from Raman measurements (figure 13). This implies that the mean free path of phonons in the samples under investigation is governed by defects smaller than the microcrystallite size. A similar effect has also been observed for the electrical conductivity in glassy carbons as a function of pyrolysis temperature [7]. Small angle X-ray scattering investigation of carbon aerogels pyrolized at temperatures up to 2100℃ reveal features that double in size from about 5 to 10 Å when the pyrolysis temperature is increased from 1500℃ to 2100℃ [21]. However, it is not clear whether the observed effect is due to a growth of micropores that are not accessible to nitrogen (see figure 10 and Table 1) or a growth of the solid phase since the scattering only reflects a combined mean value of the extension of both phases. Comparing all physical properties determined as a function of pyrolysis temperature (figures 5 through 10) reveals that none of them shows a significant change above 1500℃, in contrast to the effect observed for the thermal conductivity (figure 11). Only the features detected by small angle scattering show a comparable change in the temperature range above 1500 ℃. This is a strong hint that these are the structural entities that are responsible for the huge increase of the solid thermal conductivity with pyrolysis temperature. Future investigations have to clarify this point.

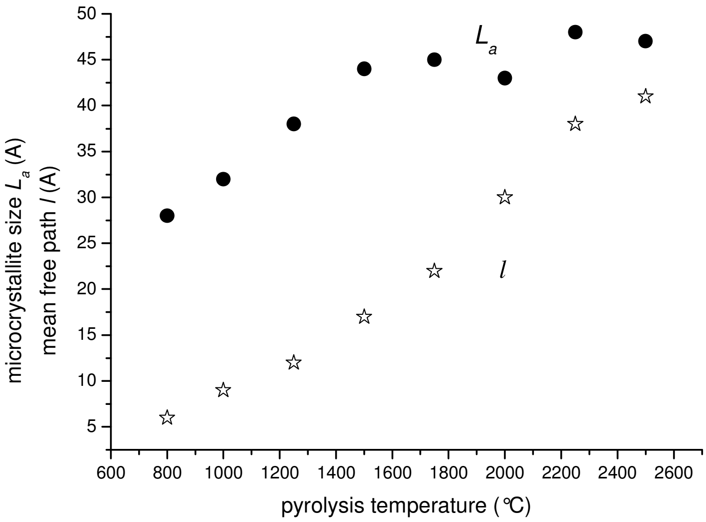

Figure 13. Microcrystallite size L_a and mean free path l calculated via equation (8) as a function of pyrolysis temperature.

6 Summary

The thermal conductivity of amorphous carbon strongly depends on the maximal treatment / pyrolysis temperature. In a pyrolysis temperature range between 800℃ and 2500℃ the thermal conductivity at 300 ℃ changes by a factor of about 8. The main cause for the observed effect can be identified to be the variation of the phonon mean free path. The phonon mean free path l is found to be systematically smaller than the microcrystallite size L_a, i.e. the mean free path is controlled by the presence of defects which are partially cured at increasing pyrolysis temperature. Small angle X-ray scattering indicates that structural changes on the length scale between 0.5 and 1 nm are the key for the drastic increase of the thermal conductivity in carbon aerogels with increasing pyrolysis temperature. An investigation of the samples presented here with small angle X-ray scattering is currently in progress.

Acknowledgements

This work has been supported by the Bavarian Science Foundation in Munich.

The authors thank Dr. M. Schreck, University of Augsburg, Germany, for performing the Raman measurements and Dr. D. Kehr, Schunk Kohlenstofftechnik GmbH, Gießen, Germany, for performing the high temperature treatment of the specimens and valuable discussions.

References

1. R. W. Pekala and F. M. Kong, “A Synthetic Route to Organic Aerogels – Mechanism, Stucture, and Properties”, 2nd International Symposium on Aerogels (ISA 2), Montpellier (France), 1989, C4-33 - 40
2. R. Saliger, “Carbon Aerogels for Application in Electrochemical Double Layer Capacitors”, Dissertation Universität Würzburg, Report E21 – 1099 -1 (1999)
3. H. Pröbstle, “Kohlenstoffaerogele für den Einsatz in Superkondensatoren”, Dissertation Universität Würzburg, Report E21 – 1001 – 1 (2001)
4. M. Wiener, “Elektroden aus Kohlenstoffaerogel für PEM-Brennstoffzellen“, Diplomarbeit Universität Würzburg, Report E21 – 1200 – 1 (2000)
5. M. Glora, “Charakterisierung von Gasdiffusionsschichten auf der Basis von Kohlenstoff-Aerogelen für PEM-Brennstoffzellen“, Dissertation Universität Würzburg, Report E21 – 0502 – 1 (2002)
6. Y. Hanzawa, H. Hatori, N. Yoshizawa, Y. Yamada, “Structural changes in carbon aerogels with high temperature treatment“, Carbon 40 (2002) 575-581
7. L. Soukup, I. Gregora and L. Jastrabik, “Raman spedtra and electrical conductiviy of glassy carbon”, Materials Science and Engeneering, B11 (1992) 355-357
8. X. Lu, O. Nilsson, J. Fricke and R. W. Pekala, *J. Appl. Phys*. **73** (1993) 583
9. O. Nilsson, V. Bock, R. Caps and J. Fricke, “High Temperature Thermal Properties of Carbon Aerogels”, Thermal conductivity **22**, Proceedings of the Twenty-Second International Conference on Thermal Conductivity, Edited by Timothy W. Tong, p. 878-887
10. V. Bock, O. Nilsson, J. Blumm, J. Fricke, “Thermal properties of carbon aerogels” *Journal of Non Crystalline Solids* 185 (1995) 233-239
11. M. Wiener, G. Reichenauer, T. Scherb, J. Fricke, „Accelerating the synthesis of carbon aerogel precursors“, Journal of Non-Crystalline Solids 350 (2004) 126-130
12. R. L. McCreery, “Carbon Electrodes: Structural Effects on Electron Transfer Kinetics”, *Electroanalytical Chemistry, A Series in Advance*, **17**, edited by A. J. Bard, Marcel Dekker, Inc., (1991) 221
13. D. S. Knight, W. B. White, “Characterisation of diamond films by Raman spectroscopy”, *Journal of Materials Research* **4** (1989) 385.
14. G.A.M. Reynolds, A.W.P. Fung, Z.H. Wang, M. S. Dresselhaus. R. W. Pekala, “The effects of external conditions on the internal structure of carbon aerogels“, *Journal of Non-Crystalline Solids* 188 (1995) 27-33.

15. J. Manara, R. Caps, F. Rather, J. Fricke, *Optics Communications* 168 (1999) 237
16. S. Brunauer, P. H. Emmett, E. Teller, *J. Am. Ceram. Soc.* **60** (1938) 309
17. O Nilsson, H Mehling, R Horn, J Fricke, R Hofmann, S G Müller, R Eckstein, D Hofmann, Determination of the thermal diffusivity and conductivity of monocrystalline silicon carbide (300-2300K), in *High Temperatures – High Pressures* **29** (1997) 73-79
18. R. D. Cowan, Pulse Method of Measuring Thermal Diffusivity at High Temperatures, J. Appl. Phys. **34** (1963) 926
19. National Bureau of Standards, *Special Publication* 260-89 (1984)
20. P. G. Klemens, *Thermal conductivity 1*, edited by R. P. Tye (Academic, London, 1969), p. 1.
21. G. Reichenauer, A. Emmerling, J. Fricke, R.W. Pekala, “Microporosity in Carbon Aerogels” , J. Non-Cryst. Solids 255 (1998) 210-214.
22. Debye, in Vorträge über die Kinetische Theorie der Materie und der Elektrizität, B. G. Teubner, Berlin, (1914) p. 43.